Experimental Assessment of a Single-layer Near-field Acoustic Holography Method in an Enclosed Space

Elias Zea, Ines Lopez Arteaga
KTH Royal Institute of Technology, The Marcus Wallenberg Laboratory for Sound and Vibration Research, Stockholm, Sweden

Summary
Planar near-field acoustic holography (PNAH) is preferably performed in anechoic spaces, since the wave-field extrapolation only holds for outgoing waves, which makes the study of certain vibro-acoustic sources a troublesome pursuit. To overcome this limitation, a number of imaging alternatives have been investigated in recent years with the use of double-layer pressure (or particle velocity) measurements, as well as of single-layer pressure and velocity measurements. Unlike these methods, our approach is to use single-layer pressure measurements and extend the PNAH method such that it is valid in the presence of a parallel reflector. In this paper we address the experimental validation of the extended PNAH formulation by means of reconstructing the pressure radiated by an omnidirectional source and exploring a few excitation frequencies. The reconstruction performance is investigated via both the free-field and the extended PNAH techniques.

PACS no. 43.60.Sx, 43.60.Pt, 43.60.Fg, 43.20.El

1. INTRODUCTION

Planar near-field acoustic holography (PNAH) is an efficient computational technique that allows contactless characterization of sound sources, by means of measuring the pressure (or velocity) in a plane parallel to such sources [1]. It is known that one of the requirements which PNAH must meet is that these sources are found in only one of the sides of the hologram [2], and due to this, the method is preferably employed in anechoic environments. An example of violation of such a requirement, which is of most interest in this paper, is the presence of a reflecting surface behind the hologram plane.

Over the years, a number of alternative techniques have been used to take into consideration the waves coming from the "wrong" side of the hologram. (Here "wrong" denotes the side opposite to that of the source plane.) Among the many approaches, we can find boundary element methods (BEM) [3], which solve the inverse problem in the spatial domain. Several other studies have made use of double-layer pressure (or particle velocity) as well as single-layer pressure and velocity (p-u) measurements [4]-[10]. In addition, double-layer BEM-based methods have been investigated [11]. Nevertheless, all these approaches exhibit a higher computational load and/or require twice as many sensors than standard PNAH.

More recently, the formulation of single-layer PNAH was extended, via a seismic model (WRW), to the case in which a parallel reflector is found at a known distance behind the hologram [12]. Briefly speaking, the WRW model solves the Rayleigh integrals via a sequence of matrix multiplications [13], and for parallel planes such multiplications can be solved sparsely in the spatial Fourier domain. In this way, it is possible to invert the Fourier-transformed equation of WRW, and use this expression for reconstructions with PNAH. The aim of the present paper is to experimentally assess the extended PNAH method and highlight the complications prone to arise in practice.

The paper is organized as follows. Section 2 presents the theory underlying the free-field and extended PNAH methods. The experimental validation is presented in Section 3, followed by a discussion of results in Section 4, and conclusions are drawn in Section 5.

2. THEORY

Throughout the remainder of the text, the time harmonic dependence $e^{j\omega t}$ is omitted.

2.1. Free-field PNAH

The theory of free-field PNAH follows from the work by Maynard and Williams [1, 2]. Here we will focus on

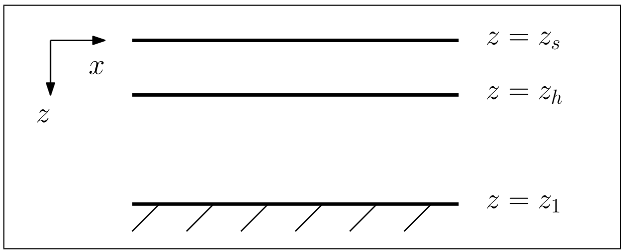

Figure 1. Geometry of the acoustic problem in the presence of a parallel reflector.

estimating the acoustic pressure at the source plane, from pressure measurements at the hologram plane. The inverse problem then follows:

$$\mathbf{P}_s = \mathbf{F}^{-1}\mathbf{G}_{sh}^{-1}\mathbf{F}\mathbf{P}_h, \tag{1}$$

where $\mathbf{F}$ is the Fourier matrix, $\mathbf{P}_s$ and $\mathbf{P}_h$ are, respectively, column vectors denoting the pressure at the source plane $z = z_s$, and hologram plane $z = z_h$; and $\mathbf{G}_{sh}$ is a diagonal matrix referred to as free-field propagator. Its elements correspond to the wavenumber coefficients of the Dirichlet Green's function characterizing the propagation from source to hologram [1]. For two parallel planes z_a and z_b, this matrix reads $\mathbf{G}_{ab} = \mathrm{diag}\{e^{\mathrm{j}\sqrt{k^2-k_x^2-k_y^2}(z_b-z_a)}\}$, where $\mathrm{j}^2 = -1$, the acoustic wavenumber is denoted with k, and the wavenumbers (k_x, k_y) discretize the spatial Fourier domain.

2.2. Extended PNAH

The extension of free-field PNAH to account for a parallel reflector was first formulated in [12]. The fundamental theory is based on the application of the WRW model in PNAH, and the geometry of the problem is illustrated in Figure 1. Here we will not derive the equations, but rather show the (modified) reconstruction expression. On mathematical grounds:

$$\mathbf{P}_s = \mathbf{F}^{-1}\left[\mathbf{I} + \mathbf{R}_1\mathbf{G}_{h1}^2\right]^{-1}\mathbf{G}_{sh}^{-1}\mathbf{F}\mathbf{P}_h, \tag{2}$$

where $\mathbf{I}$ is the identity matrix, and $\mathbf{R}_1$ is a diagonal matrix whose elements are the wavenumber coefficients of the reflectivity response of the surface. If the latter is locally reacting, it follows that $\mathbf{R}_1 = R\,\mathbf{I}$, where R is the complex reflection coefficient.

2.2.1. A note on the reflection coefficient

In practice, there may not be knowledge of the reflection coefficient beforehand. A simple way is to assume an a priori value and evaluate the reconstruction performance (see, e.g., [8] and [10]). Besides being computationally efficient (nearly indifferent with respect to free-field PNAH), this strategy preserves the convexity of the regularization functional, i.e., for a fixed reflection coefficient, the cost function remains quadratically convex, thus, the associated inverse solution is optimal and unique [14, 15]. We shall keep this note in mind for the following sections.

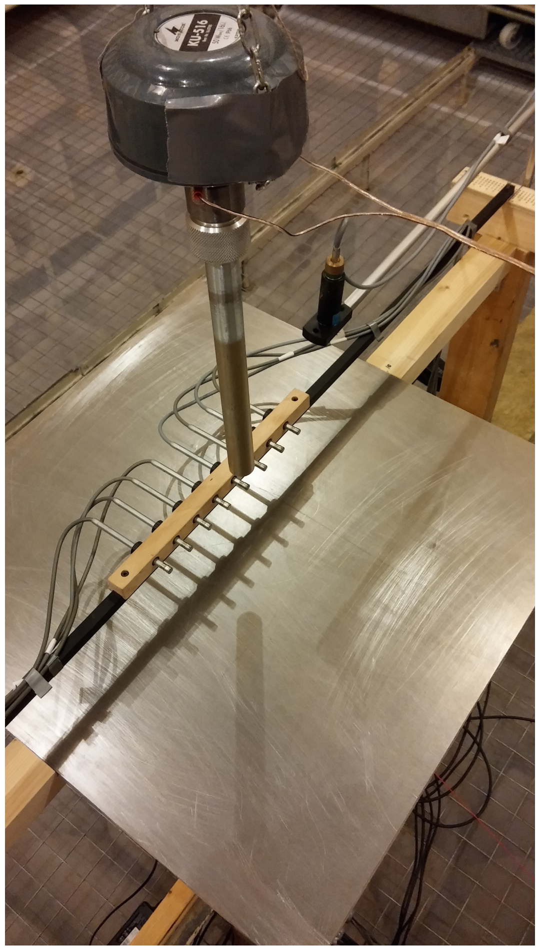

Figure 2. Photograph of experimental setup.

2.2.2. A note on bias errors

If the reflector is considered acoustically rigid, the modified propagator in Equation 2 is singular for frequencies $f \geq 0.25c/(z_1 - z_h)$, where c is the speed of sound, and wraparound errors dominate the inverse solution [16]. In few words, since the singularity demands infinitesimal sampling of wavenumber space, the inverse solution consists of infinitely many replicas of itself [1]. As a matter of fact this phenomenon is not new, and it has been encountered in double-layer array methods, e.g., estimation of reflection coefficients and field separation techniques [8]. A typical solution to alleviate wraparound is to average the wavenumber spectrum of the propagating operator near the singularity [17, 18].

3. EXPERIMENTAL STUDY

A photograph of the experimental setup can be found in Figure 2. All measurements are performed in an anechoic chamber. A line array of eight B&K 4260 microphones is used and the data is acquired with B&K PULSE (via a VXI E1432A system) with sampling frequency of 5 [kHz]. (The microphones are calibrated in an impedance tube excited with plane waves within a 4.5 [kHz] bandwidth.) The line array is manually shifted such as to have a total amount of 24 x 16 measurement points, giving a measurement aperture of 0.24 x 0.16 [m^2]. The distance from the source plane to the hologram plane is 2 [cm], and the distance from the hologram plane to the reflector is 8.5 [cm]. (For these distances, $c \simeq 340$ [m/s] and an acoustically rigid reflector, the modified propagator is singular for $f \simeq 1000$.) The reflector consists of a steel sheet of dimensions 0.5 x 0.5 [m^2] and thickness 2 [mm], and it is mounted above a wood layer of 8 [mm] thickness. The acoustic source consists of an omnidirectional point-like source centered in the measurement aperture and positioned 5 [cm] away from the source plane. The frequencies of interest are f = 400, 800, 1000, 1250, 1600, 2000, 2500 and 3150 [Hz]. In order to obtain the phase information at the measurement points a reference microphone is placed in the vicinity of the source. The reconstructions are performed via the free-field and the extended PNAH methods, and the ground-truth source pressure is measured in the absence of the reflector.

In order to quantify the reconstruction performance of the PNAH methods, we compute the reconstruction error in decibels as follows

$$\mathrm{E} = 20\log\frac{\|\mathbf{P}_s^{\mathrm{r}} - \mathbf{P}_s^{\mathrm{g}}\|}{\|\mathbf{P}_s^{\mathrm{g}}\|}, \tag{3}$$

where $\|\cdot\|$ is the Euclidean norm of the vector, and superscripts r and g denote, respectively, reconstructed and ground-truth source pressure.

3.1. Signal pre-processing and conditioning

For the chosen measurement aperture, the propagating content for $f \lesssim 1430$ [Hz] only consists of waves with normal incidence angle (i.e., $k_z = k$). Therefore, the hologram measurements are extrapolated via basic border padding [19] to an aperture of 1.28 x 1.28 [m^2]. A Tukey window is used to periodize the hologram data, and the spatial decay rate is $\phi(x, y) = (0.8125, 0.875)$, which is considered overall appropriate in our reconstructions. One could argue that border padding and large (smooth) window decay rates are adequate since the source has a point-like behavior, and it is positioned in the center of the aperture. On the other hand, for the purpose of regularization we use the modified exponential filter, and the filter parameters are found via wavenumber-based generalized cross-validation (GCV) [20]. The domain of the GCV function consists of 31 cut-off wavenumbers and 11 slopes. The choice of regularization strategy is based upon empirical observation.

4. RESULTS

It is now opportune to recall the above note on the complex reflection coefficient. Instead of choosing one

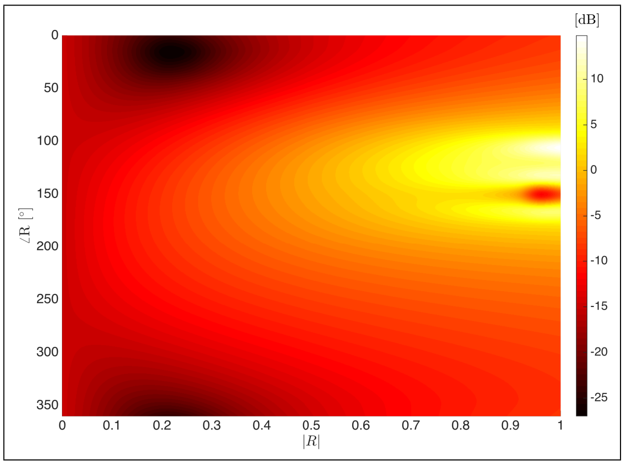

Figure 3. Reconstruction error as a function of magnitude and phase of reflection coefficient at $f = 400$ [Hz]. Global minimum is -26.87 [dB] at coefficient $R = 0.208\,\mathrm{e}^{\mathrm{j}\pi/12}$.

value for all reconstructions, we define a set of 625 reflection coefficients spanning the unit circle of the complex plane, and iteratively compute the reconstruction errors at each frequency. The reflector is modelled as an infinitely large locally reacting surface. In essence, the error of extended PNAH is computed as a function of the complex reflection coefficient, i.e. $E(R)$. An instance of this function can be found in Figure 3, where the left-most region (null coefficient) corresponds with free-field PNAH, and the overall minimum value corresponds with the optimal coefficient via extended PNAH. Also, wraparound errors can be seen in the right-most region.

Table I shows the frequency-dependent optimal reflection coefficients $\hat{R} = \mathrm{argmin}_R\, E(R, f)$, provided f is fixed. It is worth noting that, for $f \gtrsim 1000$ [Hz] and the given problem parameters, $\hat{R}$ is never unity since solutions with wraparound errors cannot yield a global minimum. As a matter of fact, these optimal coefficients include the modelling effects due to finite aperture, extrapolation and regularization. Therefore they do not necessarily correspond with the actual (physical) reflection coefficient of the steel sheet, but yield optimal reconstruction via extended PNAH.

Figure 4 shows the source reconstructions and the associated errors for all frequencies under study. Overall, we can see that extended PNAH improves the reconstruction accuracy with respect to free-field PNAH at all frequencies. Diffraction due to the line array can be observed for frequencies higher than 2000 [Hz]. (For $f = 3150$ [Hz] the pressure field is severely distorted.) This is particularly noticeable in the pressure values at the bottom of the measurement aperture (see Figure 4), and it was attributed to the distortion due to the microphone holder (see Figure 1) whose size is $s = 2$ [cm] wide. Since the presence of the holder was not taken into account in the calibration transfer functions, the pressure fields are distorted for acoustic wavelengths $\lambda \lesssim 10s = 20$ [cm]. A straightforward

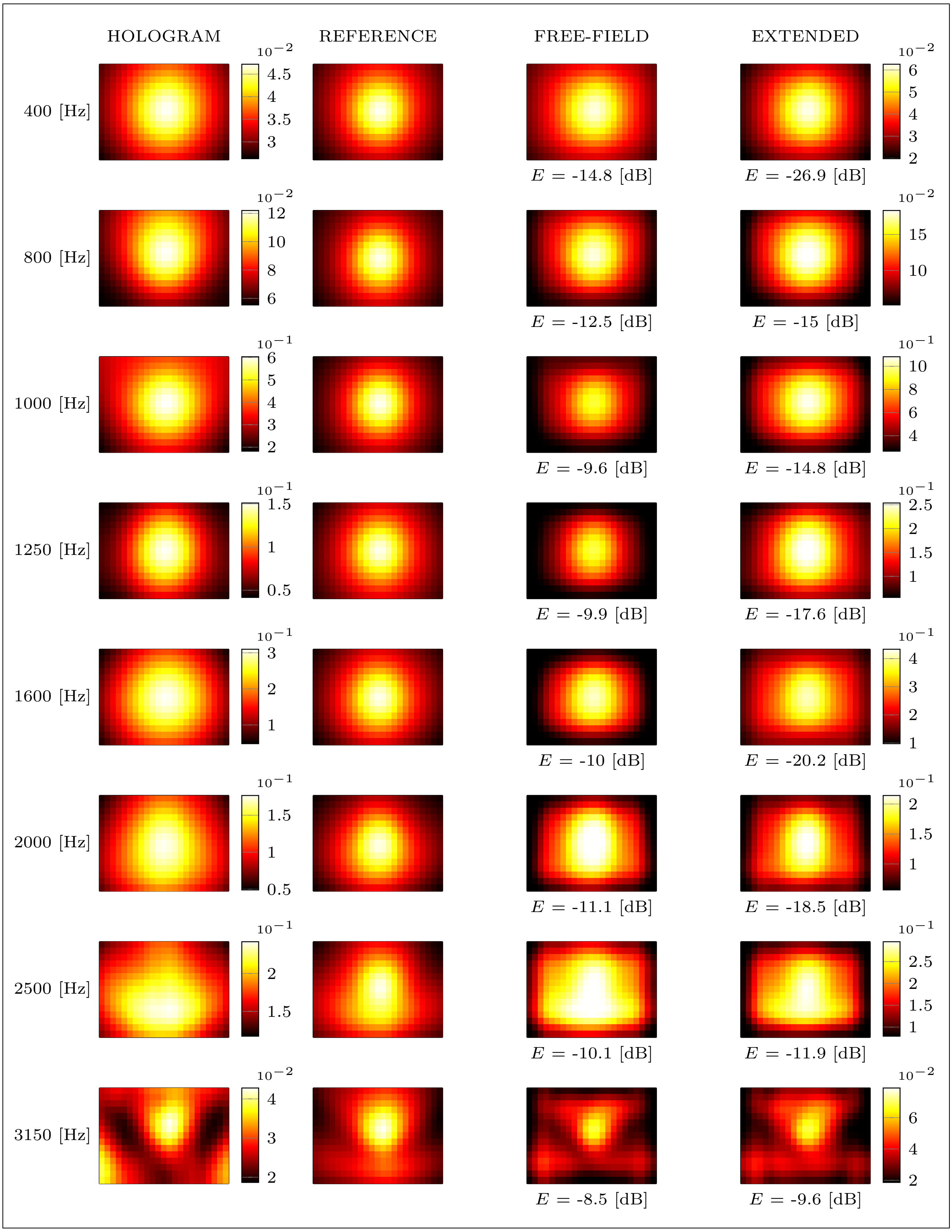

Figure 4. Source reconstructions and associated errors for all frequencies under study. Left-most column: Hologram pressure. Left-center column: Reference (ground-truth) source pressure. Right-center column: Source pressure reconstructed via free-field PNAH. Right-most column: Source pressure reconstructed via extended PNAH. The plots show the magnitude of the pressure field in units of [Pa].

Table I. Optimal complex reflection coefficients used for the reconstructions via extended PNAH.

f [Hz]	$\|\hat{R}\|$	$\angle\hat{R}\,[^\circ]$
400	0.208	15
800	0.292	-30
1000	0.54	-30
1250	0.875	-15
1600	0.792	-45
2000	0.625	-45
2500	0.417	-45
3150	0.583	45

solution would be to calibrate the microphones held in the line array, such that the the effect of diffraction is taken into account in the calibration functions.

Lastly, we would like to stress that the reconstruction errors with extended PNAH in Figure 4 are obtained with the optimal coefficients from Table I, and the latter require the knowledge of the free-field source pressure. Therefore, an accurate estimate of the reflection coefficient is needed in order to successfully apply the extended PNAH method for source identification.

5. CONCLUSIONS

The validity of an extended PNAH method for sound source identification in the presence of a parallel reflector is experimentally assessed. If an accurate estimate of the reflection coefficient is given, the extended method offers the possibility to improve the reconstruction performance, with respect to free-field PNAH, of sources radiating in the presence of a parallel reflector. In addition, extended PNAH is formulated in wavenumber space and only requires a single-layer hologram measurement, which is advantageous over existing methods. This suggests further investigation should be done regarding extended PNAH with unknown reflection coefficient.

Acknowledgement

The present work is financially supported by the Swedish Research Council (Vetenskapsrådet).

References

[1] J. D. Maynard, E. G. Williams, Y. Lee: Nearfield acoustic holography: I. Theory of generalized holography and the development of NAH. J. Acoust. Soc. Am. **78**, 1395–1413 (1985).

[2] E. G. Williams: Fourier Acoustics Sound Radiation and Nearfield Acoustical Holography. Academic Press, UK (1999).

[3] B.-K. Kim, J.-G. Ih: On the reconstruction of the vibro-acoustic field over the surface enclosing an interior space using the boundary element method. J. Acoust. Soc. Am. **100**, 3003–3016 (1996).

[4] J. Hald: Patch holography in cabin environments using a two-layer handheld array with extended SONAH algorithm. Proc. Euronoise, Finland (2006).

[5] F. Jacobsen, V. Jaud: Statistically optimized near field acoustic holography using an array of pressure-velocity probes. J. Acoust. Soc. Am. **121**, 1550–1558 (2007).

[6] E. Fernandez-Grande, F. Jacobsen: Sound field separation with a double layer velocity transducer array. J. Acoust. Soc. Am. **130**, 5–8 (2011).

[7] E. Fernandez-Grande, F. Jacobsen, Q. Leclère: Sound field separation with sound pressure and particle velocity measurements. J. Acoust. Soc. Am. **132**, 3818–3825 (2012).

[8] D.-Y. Hu, C.-X. Bi, Y.-B. Zhang, L. Geng: Extension of planar near field acoustic holography for sound source identification in a noisy environment. J. Sound and Vibration **333**, 6395–6404 (2014).

[9] Z. Havránek, P. Beneš, S. Klusáček: Comparison of patch acoustic holography methods for confined space. Proc. Inter-Noise, Australia (2014).

[10] C.-X. Bi, D.-Y. Hu, Y.-B. Zhang, W.-Q. Jing: Identification of active sources inside cavities using the equivalent source method-based free-field recovery technique. J. Sound and Vibration (2015), http://dx.doi.org/10.1016/j.jsv.2015.02.023.

[11] C. Langrenne, M. Melon, A. Garcia: Measurement of confined acoustic sources using near-field acoustic holography. J. Acoust. Soc. Am. **126**, 1250–1256 (2009).

[12] E. Zea, I. Lopez Arteaga: A single-layer formulation of Fourier-based planar NAH for enclosed spaces. Proc. Forum Acusticum, Krakow (2014).

[13] A. J. Berkhout, D. de Vries, J. Baan, B. W. van den Oetelaar: A wave field extrapolation approach to acoustical modeling in enclosed spaces. J. Acoust. Soc. Am. **105**, 1725–1733 (1999).

[14] E. G. Williams: Regularization methods for near-field acoustical holography. J. Acoust. Soc. Am. **110**, 1976–1988 (2001).

[15] S. Boyd, L. Vandenberghe: Convex Optimization. Cambridge University Press, UK (2004).

[16] E. Zea, I. Lopez Arteaga: Extended single-layer planar near-field acoustic holography for identification of sound sources in the presence of a parallel reflector. Submitted.

[17] E. G. Williams, J. D. Maynard: Numerical evaluation of the Rayleigh integral for planar radiators using the FFT. J. Acoust. Soc. Am. **72**, 2020–2030 (1982).

[18] M.-T., Cheng, J. A. Mann III, A. Pate: Wavenumber domain separation of the incident and scattered sound field in Cartesian and cylindrical coordinates. J. Acoust. Soc. Am. **97**, 2293–2303 (1995).

[19] I. Lopez Arteaga, R. Scholte, H. Nijmeijer: Improved source reconstruction in Fourier-based Near-field Acoustic Holography applied to small apertures. Mechanical Systems and Signal Processing **32**, 359–373 (2012).

[20] R. Scholte, I. Lopez Arteaga, N. B. Roozen, H. Nijmeijer: Wavenumber domain regularization for near-field acoustic holography by means of modified filter functions and cut-off and slope iteration. Acta Acustica, **94**, 339–348 (2008).